Inclusive photoproduction of strange baryons at 20 GeV

K. Abe,[m] R. Armenteros,[k,*] T. C. Bacon,[e] J. Ballam,[k] H. H. Bingham,[o] J. E. Brau,[q] K. Braune,[k] D. Brick,[b] W. M. Bugg,[q] J. M. Butler,[k] W. Cameron,[e] H. O. Cohn,[i] D. C. Colley,[a] S. Dado,[l] R. Diamond,[d,†] P. Dingus,[o] R. Erickson,[k] R. C. Field,[k] B. Franek,[j] N. Fujiwara,[h] T. Glanzman,[k] I. M. Godfrey,[e] J. J. Goldberg,[l] A. T. Goshaw,[c] G. Hall,[e] E. R. Hancock,[j] T. Handler,[q] H. J. Hargis,[q] E. L. Hart,[q] M. J. Harwin,[e] K. Hasegawa,[m] R. I. Hulsizer,[g] M. Jobes,[a] T. Kafka,[n] G. E. Kalmus,[j] D. P. Kelsey,[j] T. Kitagaki,[m] A. Levy,[p] P. W. Lucas,[c,‡] W. A. Mann,[n] R. Merenyi,[n] R. Milburn,[n] C. Milstene,[p] K. C. Moffeit,[k] A. Napier,[n] S. Noguchi,[h] F. Ochiai,[f] S. O'Neale,[a] A. P. T. Palounek,[c] I. A. Pless,[g] P. Rankin,[k] W. J. Robertson,[c] H. Sagawa,[m] T. Sato,[f] J. Schneps,[n] S. J. Sewell,[j] J. Shank,[o] A. M. Shapiro,[b] R. Sugahara,[f] A. Suzuki,[f] K. Takahashi,[f] K. Tamai,[m] S. Tanaka,[m] S. Tether,[g] D. A. Waide,[a] W. D. Walker,[c] M. Widgoff,[b] C. G. Wilkins,[a] S. Wolbers,[o,‡] A. Yamaguchi,[m] R. K. Yamamoto,[g] S. Yamashita,[h] Y. Yoshimura,[f] G. P. Yost,[o] and H. Yuta[m]

[a]*Birmingham University, Birmingham, B15 2TT, England*
[b]*Brown University, Providence, Rhode Island 02912*
[c]*Duke University, Durham, North Carolina 27706*
[d]*Florida State University, Tallahassee, Florida 32306*
[e]*Imperial College, London, SW7 2BZ, England*
[f]*National Laboratory for High Energy Physics (KEK), Oho-machi, Tsukuba-gun, Ibaraki 305, Japan*
[g]*Massachusetts Institute of Technology, Cambridge, Massachusetts 02139*
[h]*Nara Womens University, Kita-uoya, Nishi-Machi Nara 630, Japan*
[i]*Oak Ridge National Laboratory, Oak Ridge, Tennessee 37830*
[j]*Rutherford Appleton Laboratory, Didcot, Oxon OX11 OQX, England*
[k]*Stanford Linear Accelerator Center, Stanford University, Stanford, California 94305*
[l]*Technion-Israel Institute of Technology, Haifa 32000, Israel*
[m]*Tohoku University, Sendai 980, Japan*
[n]*Tufts University, Medford, Massachusetts 02155*
[o]*University of California, Berkeley, California 94720*
[p]*University of Tel Aviv, Tel Aviv, Israel*
[q]*University of Tennessee, Knoxville, Tennessee 37916*

(Received 3 May 1985)

Cross sections are presented for the inclusive photoproduction of K_S^0, Λ, $\bar{\Lambda}$, Ξ^-, $\bar{\Xi}^-$, Σ^0, and $\Sigma^{*\pm}(1385)$ at 20 GeV. An upper limit to Ω^- production is also given. The data come from 284 000 hadronic events photoproduced in the SLAC 1-m hydrogen-bubble-chamber hybrid facility exposed to a nearly monochromatic, polarized 20-GeV backscattered photon beam. A comparison of the K_S^0, Λ, $\bar{\Lambda}$, and Ξ^- rates per inelastic event to $\pi^\pm p$ data show that γp rates are consistent with being higher than the $\pi^\pm p$ rates, providing evidence of an $s\bar{s}$ component of the photon. The pair cross sections for $K_S^0K_S^0$, $K_S^0\Lambda$, $K_S^0\bar{\Lambda}$, and $\Lambda\bar{\Lambda}$ are presented. The x_F distributions of the Λ, $\bar{\Lambda}$, and Ξ^- are compared to a quark-diquark fusion model, giving information on strange-baryon photoproduction mechanisms.

I. INTRODUCTION

We report here cross sections and Feynman-x distributions for the inclusive photoproduction on hydrogen of strange baryons at 20 GeV. Cross sections are presented also for pairs of neutral strange particles. Comparison with analogous $\pi^\pm p$ production of strange baryons and with predictions of a quark-diquark fusion model give information on the production mechanisms of strange baryons. Our experiment is the first to measure inclusive K_S^0, Λ, $\bar{\Lambda}$, $\Sigma^*(1385)$, and Ξ^- photoproduction across the entire range of x_F. We have previously published[1] results on K_S^0, Λ, and $\bar{\Lambda}$ photoproduction based on $\sim\frac{1}{3}$ of our present statistics.

The paper is organized as follows. We first describe the experiment in Sec. II. Single and pair cross sections are given in Sec. III and compared with available $\pi^\pm p$ data. In Sec. IV we present the x_F distributions and compare them with fits to a quark-diquark fusion model. Conclusions are given in Sec. V.

II. EXPERIMENTAL PROCEDURE

Our data come from SLAC BC72/73, an exposure of the SLAC hybrid facility (SHF) (see Fig. 1) to a 20-GeV linearly polarized γ beam. The SHF consisted of the 1-m diameter hydrogen bubble chamber, in a 2.6-T magnetic field, cycling at 10—12 Hz, whose flash was triggered on evidence for a hadronic interaction in the hydrogen. This evidence was provided by three planes of proportional wire chambers (PWC) tracking charged particles down-

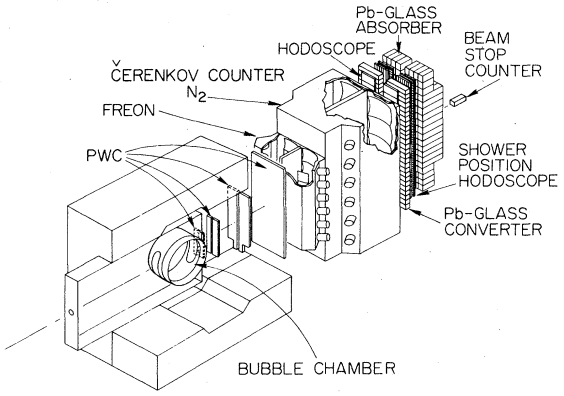

FIG. 1. The SLAC hybrid facility showing the bubble chamber and the downstream detectors.

stream of the bubble chamber or by a lead-glass wall (LGW) detecting energetic γ-ray showers, electrons and charged hadrons. Two Čerenkov counters between the PWC's and the LGW provided some $\pi/K/p$ identification (unused in this study). The γ beam was produced by backscattering 4.68-eV laser light from the SLAC 30-GeV electron beam. Selection of γ rays scattered almost directly backwards produced a beam spectrum in the SHF peaked at 20 GeV with a full width at half maximum (FWHM) of ~ 2 GeV. The beam flux and spectrum were monitored by a pair spectrometer upstream of the bubble chamber and a lead-lucite beam-stop shower counter downstream. See Refs. 1 and 2, and references therein for further details.

III. CROSS SECTIONS

A. Data sample

The present study is based on measurements of 284 000 hadronic photoproduction events found in a total of 2.4×10^6 photographs taken. The film was scanned for hadronic events [and a special search was made for charmed and strange particle decays near the production vertex, using a special high-resolution (~ 50-μm) view]. The events were measured and processed through geometry and kinematics programs, checked for errors, and a summary of information on each event was written onto data summary tapes (DST's).

Fiducial cuts are made on both the primary vertex and the V^0 vertices' positions in the bubble chamber. The primary vertex must be contained in a cylinder with radius 3 mm and axis along the beam direction and also must be in the region $-45 < x < 30$ cm, where x is the coordinate along the beam. (The bubble chamber is from $-50 < x < 50$ cm along the beam line.) The V^0 fiducial volume was defined to be a cylinder with radius 43 cm and axis at $x = -2$ cm inside the 50-cm-radius bubble chamber.

B. K_S^0, Λ, and $\bar{\Lambda}$ cross sections

1. Event selection

There were $\sim 45\,000$ V^0's measured in this experiment. The procedure for event selection is similar to that of Ref. 1 and the details may be found in Ref. 2. The V^0's were fit to the following four hypotheses using the kinematic-fitting programs SQUAW, GRIND, or Rutherford Kinematics.

$$\gamma p \rightarrow (p) e^+ e^- ,$$
$$K_S^0 \rightarrow \pi^+ \pi^- ,$$
$$\Lambda \rightarrow p \pi^- ,$$
$$\bar{\Lambda} \rightarrow \bar{p} \pi^+ .$$

As a first step in resolving the ambiguities, the γ's were removed as follows: The invariant mass of each V^0 when interpreted as an e^+e^- pair was calculated. The transverse momentum p_t of the e^+ with respect to the V^0 flight path was also computed. If $M_{e^+e^-} < 30$ MeV/c^2 or $p_t < 10$ MeV/c, the V^0 was called a γ and removed. Monte Carlo studies estimate that less than 1% of K_S^0, Λ, or $\bar{\Lambda}$ was lost by this cut. An additional cut on the p_t of the e^- removed an insignificant additional number of γ's and this cut was not used. After the γ's were removed, there were 21 895 V^0's left. Of these, 16 885 (77%) fit only one hypothesis with three constraints (3C) and $P(\chi^2) > 0.1\%$. 2536 (12%) V^0's fit more than one hypothesis, and 2474 (11%) fit no hypotheses.

The 2536 ambiguities were resolved statistically using the following procedure. (1) A K_S^0/Λ ambiguity was resolved as a K_S^0 if the [$P(\chi^2)$ of $K_S^0 \rightarrow \pi^+\pi^-$] was greater than 0.70 and [$P(\chi^2)$ of $K_S^0 > P(\chi^2)$ of Λ]. Otherwise it was called a Λ. (2) A $K_S^0/\bar{\Lambda}$ ambiguity was resolved as an $\bar{\Lambda}$ if [$P(\chi^2)$ of $\bar{\Lambda}$] was greater than 0.90 and [$P(\chi^2)$ of $\bar{\Lambda} > P(\chi^2)$ of K_S^0]; otherwise it was called a K_S^0. This somewhat arbitrary procedure was designed to produce the correct numbers of K_S^0, Λ, $\bar{\Lambda}$ statistically, as revealed, for example, by distributions approximately flat in $\cos\theta_{\text{c.m.}}$ as discussed below. The exact values of the χ^2 cuts are not critical. Table I lists the V^0's as they are identified to this point.

The 2474 unidentified V^0's were analyzed using kinematic fits with fewer than three constraints. The origins of these V^0's are the following. They may be legitimate V^0's associated with the event that do not give 3C fits due to the interaction of the neutral particle in the hydrogen or due to the decay or the interaction in the hydro-

TABLE I. Identification of V^0's after separation with 3C fits.

Unidentified	2 474
γ	20 674
K_S^0 unique	11 418
Λ unique	5 216
$\bar{\Lambda}$ unique	251
K_S^0/Λ ambiguous	1 975
$K_S^0/\bar{\Lambda}$ ambiguous	559
$\Lambda/\bar{\Lambda}$ ambiguous	2
Total	42 569
K_S^0/Λ resolved as K_S^0	412
$K_S^0/\bar{\Lambda}$ resolved as K_S^0	471
K_S^0/Λ resolved as Λ	1 563
$K_S^0/\bar{\Lambda}$ resolved as $\bar{\Lambda}$	88

gen of either of the charged tracks produced in the V^0 decay. They may not be emitted from the primary vertex of the event; i.e., they could come from secondary interactions in the event, window interactions, or other events in the chamber. They could be K_L^0 or other three-body decays, or they may be badly measured.

The above-mentioned causes for 3C failures were investigated and some of the 2C, 1C and 0C fits were apportioned to K_S^0, Λ, and $\bar{\Lambda}$. There were 767 ± 39 K_S^0, 536 ± 38 Λ, and 36 ± 13 $\bar{\Lambda}$ found. The rest were assumed to be unassociated V^0's, K_L^0, etc. The details of the no-fit analysis are found in Ref. 2.

Summing the 3C and the resolved no-fit samples, the total (unweighted) numbers of K_S^0, Λ, and $\bar{\Lambda}$ in the fiducial volume are given in Table II.

The samples of K_S^0, Λ, and $\bar{\Lambda}$ were checked for possible contamination and biases by checks on the mass, $\cos\theta_{\text{c.m.}}$ and lifetimes. The masses of the V^0's from the measured track quantities, interpreted as $\pi^+\pi^-$, $p\pi^-$, and $\bar{p}\pi^+$ are shown in Fig. 2 for all possible combinations and for the final 3C fit samples. The widths are consistent with the experimental resolution. All three distributions peak at the correct mass value and show no apparent background or biases.

The angle $\theta_{\text{c.m.}}$ is defined as the angle between the direction of the positive decay track in the rest frame of the V^0 and the direction of the V^0 in the laboratory frame. That is,

$$\cos\theta_{\text{c.m.}} = \frac{\mathbf{p}^+_{\text{c.m.}} \cdot \mathbf{p}_{V_0}}{|\mathbf{p}^+_{\text{c.m.}}|\,|\mathbf{p}_{V^0}|} .$$

The $\cos\theta_{\text{c.m.}}$ distributions for the 3C K_S^0, Λ, and $\bar{\Lambda}$ passing cuts are shown in Fig. 3. These distributions are approximately flat in $\cos\theta_{\text{c.m.}}$ as predicted, justifying the values of $P(\chi^2)$ used to separate the V^0's.

The mean lifetimes were determined by a maximum-likelihood method and are 2.686 ± 0.033, 7.78 ± 0.12, and 8.43 ± 0.98 cm for the $c\tau$ of the K_S^0, Λ, and $\bar{\Lambda}$ samples,

TABLE II. Cross sections presented in this paper. The errors include statistical and systematic errors. The cross sections include strange baryons produced indirectly, e.g., Λ from the decay of Σ^0.

Particle	Unweighted number	$\sigma(\mu b)$
K_S^0	13068 ± 121	9.663 ± 0.272
Λ	7315 ± 93	5.603 ± 0.180
$\bar{\Lambda}$	375 ± 23	0.389 ± 0.036
Ξ^-	73 ± 9	0.117 ± 0.017
$\bar{\Xi}^-$	9 ± 4	0.010 ± 0.004
Σ^0	29 ± 8	1.65 ± 0.44
$\Sigma^{*+}(1385)$	208 ± 19	0.63 ± 0.06
$\Sigma^{*-}(1385)$	109 ± 15	0.33 ± 0.05
Ω^-	<7.3 at 90% CL	<0.017 at 90% CL
$K_S^0K_S^0$	467 ± 22	0.973 ± 0.040
$K_S^0\Lambda$	366 ± 19	1.125 ± 0.059
$K_S^0\bar{\Lambda}$	6 ± 2	0.023 ± 0.009
$\Lambda\bar{\Lambda}$	11 ± 3	0.126 ± 0.038
$\Lambda\Lambda$	4 ± 2	0.028 ± 0.014

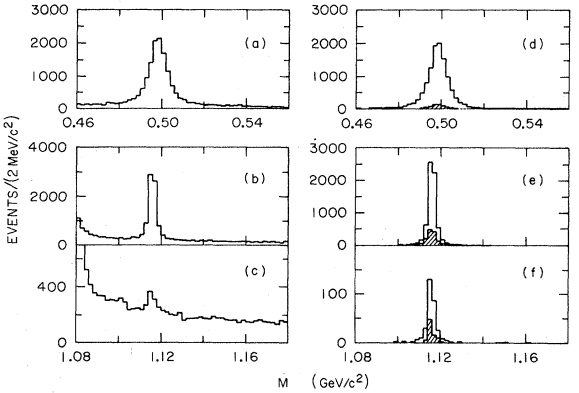

FIG. 2. Invariant-mess combinations of V^0's. (a) $M_{\pi^+\pi^-}$ of all V^0's; (b) $M_{p\pi^-}$ of all V^0's; (c) $M_{\bar{p}\pi^+}$ of all V^0's (d) $M_{\pi^+\pi^-}$ of 3C K_S^0; (e) $M_{p\pi^-}$ of 3C Λ; (f) $M_{\bar{p}\pi^+}$ of 3C $\bar{\Lambda}$. The shaded portions on (d), (e), and (f) are from the resolved 3C V^0's.

respectively, and $(\tau_\Lambda-\tau_{\bar{\Lambda}})/(\tau_\Lambda+\tau_{\bar{\Lambda}})=-0.040\pm0.063$. These agree well with the Particle Data Group[3] (PDG) values of 2.675 ± 0.007 cm for K_S^0 and 7.89 ± 0.06 cm for Λ and $(\tau_\Lambda-\tau_{\bar{\Lambda}})/(\tau_\Lambda+\tau_{\bar{\Lambda}})=0.044\pm0.085$.

2. K_S^0, Λ, and $\bar{\Lambda}$ cross sections

From the sample of K_S^0, Λ, and $\bar{\Lambda}$ events the inclusive cross sections were calculated. The weighted number of V^0's was normalized to the total number of hadronic events in the sample to compute the inclusive cross sections. Corrections were made for the following effects with the average value of the correction in parentheses for K_S^0, Λ, and $\bar{\Lambda}$: the relative efficiency for detecting events with V^0 to detecting all hadronic events (0.968, 0.971, 0.969), losses due to the finite length of the bubble-chamber fiducial volume (1.204, 1.167,1.414), losses in the azimuthal angle of the V^0 decay (1.037, 1.025, 1.08), decay branching ratios of the $K_S^0\to\pi^+\pi^-$, $\Lambda\to p\pi^-$, and $\bar{\Lambda}\to\bar{p}\pi^+$ (0.686, 0.642, 0.642). The total hadronic pho-

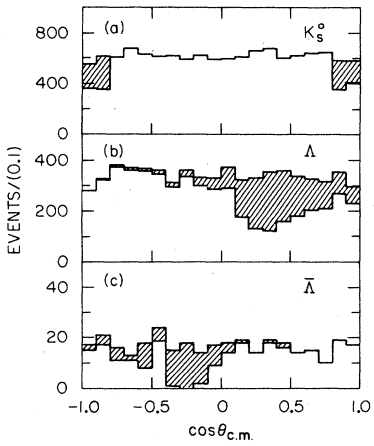

FIG. 3. $\cos\theta_{\text{c.m.}}$ distributions for 3C unique plus resolved (a) K_S^0; (b) Λ; (c) $\bar{\Lambda}$. The shaded portions are the resolved 3C V^0 contributions.

toproduction cross section, 115 ± 2 μb, was taken from another photoproduction experiment.[4]

The resulting inclusive cross sections for K_S^0, Λ, and $\bar{\Lambda}$ production are presented in Table II and are consistent with previously published cross sections measured in this experiment.[1]

3. *Comparison to γp and $\pi^{\pm}p$ data*

Data on inclusive K_S^0, Λ, and $\bar{\Lambda}$ photoproduction are very scarce. Earlier measurements of neutral strange particle photoproduction include a measurement[5] of exclusive final states (e.g., $K_S^0\Lambda$) at 5.8 GeV and a measurement of the total visible strange topology (kinks and V^0's visible in the bubble chamber) at 9.3 GeV.[6] Neither of these experiments measured the inclusive production of K_S^0, Λ, or $\bar{\Lambda}$. Our experiment is the first γp experiment to measure inclusive K_S^0, Λ, or $\bar{\Lambda}$ production across the entire x_F range.

A much more recent experiment at higher photon energies done by the CERN Ω collaboration has studied inclusive Λ and $\bar{\Lambda}$ photoproduction in the energy range 25—70 GeV.[7] However, the total inclusive Λ and $\bar{\Lambda}$ cross sections were not measured in the CERN Ω experiment because backward Λ and $\bar{\Lambda}$ ($x_F<-0.2$) were not within the detector acceptance or were removed by the data analysis chain and therefore were lost. This is a very serious problem for the Λ especially, as most of the cross section is at $x_F<-0.2$.

Many $\pi^{\pm}p$ and $\pi^{\pm}d$ experiments have measured inclusive K_S^0, Λ, and $\bar{\Lambda}$ production. A comparison of the number of K_S^0, Λ, and $\bar{\Lambda}$ per inelastic event, as a function of the available energy, may reveal information about the nature of the photon (in particular, the size of the $s\bar{s}$ component and how this component couples to the final state). This comparison requires some interpretation and assumptions. For the $\pi^{\pm}p$ data, the available energy is defined to be $E_A=\sqrt{s}-m_p-m_\pi$, whereas in the γp case we take $E_A=\sqrt{s}-m_p$. The definition of the inelastic cross section for the γp case is not nearly as straightforward as for the $\pi^{\pm}p$ case, where the elastic reaction $\pi^{\pm}p\to\pi^{\pm}p$ is measured and subtracted from the total cross section to give the inelastic cross section. It is believed that the photon usually couples to a vector meson before interacting hadronically with the proton target. This is the basis of the vector-meson-dominance model (VDM).[8] This can be taken to mean that the reaction $\gamma p\to Vp$ may be regarded as an elastic reaction (where V=a vector meson). Subtraction of this cross section reduces the inelastic cross section used in the calculation. The largest contributions to $\gamma p\to Vp$ are the vector mesons ρ, ω, and ϕ, with smaller contributions from the $p'(1600)$ and other excited states. The $\gamma p\to\rho p$ "elastic" cross section is 10.8 ± 1.1 μb, as measured in this experiment.[9] We subtract only the ρ contribution to arrive at an inelastic cross section of $\sigma_{\text{inel}}=104.2$ μb.

The results are shown in Table III and Figs. 4, 5, and 6. The line drawn on each plot is a least-squares fit to all the π^+p and π^-p data. The χ^2/DF are 72/14, 74/17, 42/13, and 0.524/1 for K_S^0, Λ, $\bar{\Lambda}$, and Ξ^-, suggesting that the $\pi^{\pm}p$ data are not very consistent (Ξ^- is discussed below). The γp points are all above the πp data fit. However, there is a large spread to the $\pi^{\pm}p$ data, reflecting the large systematic errors. Naively, we would expect the γp data to be on the order of 10% higher than the πp data because the photon contains a valence $s\bar{s}$ component which the π

TABLE III. Number of V^0 per inelastic event for various π^+p, π^-p experiments and this experiment.

Beam	Beam energy (GeV)	E_A (GeV)	$\sigma_{K_S^0}/\sigma_{\text{inel}}$	$\sigma_\Lambda/\sigma_{\text{inel}}$	$\sigma_{\bar{\Lambda}}/\sigma_{\text{inel}}$	Reference
π^+	5	2.13		0.026±0.002		19
π^+	16	4.48	0.077±0.004	0.044±0.003	0.0027±0.0004	20
π^+	18.5	4.89	0.058±0.004	0.037±0.003	0.0022±0.0002	21
π^+	32	6.73	0.105±0.007	0.051±0.005	0.0072±0.0018	22
π^+	100	12.7	0.205±0.020	0.055±0.010	0.0075±0.0040	23
π^+	147	16.6	0.200±0.015	0.090±0.010	0.0349±0.0050	24
π^-	1.23	0.722		0.011±0.003		25
π^-	6	2.41	0.043±0.003	0.041±0.003		26
π^-	11.4	3.64	0.092±0.020	0.035±0.012		27
π^-	15	4.31	0.091±0.004	0.059±0.003	0.0023±0.0003	28
π^-	16	4.48	0.071±0.004	0.042±0.003	0.0019±0.0002	29
π^-	18.5	4.89	0.075±0.005	0.044±0.004	0.0029±0.0003	21
π^-	40	7.64		0.069±0.014	0.0066±0.0014	30
π^-	100	12.7	0.143±0.005	0.075±0.004	0.0186±0.0029	31
π^-	147	16.6	0.175±0.018	0.079±0.010	0.0181±0.0062	32
π^-	200	18.3	0.178±0.012	0.073±0.006	0.0205±0.0029	31
π^-	205	18.6	0.173±0.029	0.081±0.016	0.0281±0.0109	33
π^-	250	20.6	0.189±0.032	0.070±0.009	0.0195±0.0043	34
π^-	360	24.9	0.210±0.011	0.075±0.010	0.0222±0.0033	31
γ	19.5	5.18	0.093±0.003	0.054±0.002	0.0037±0.0003	

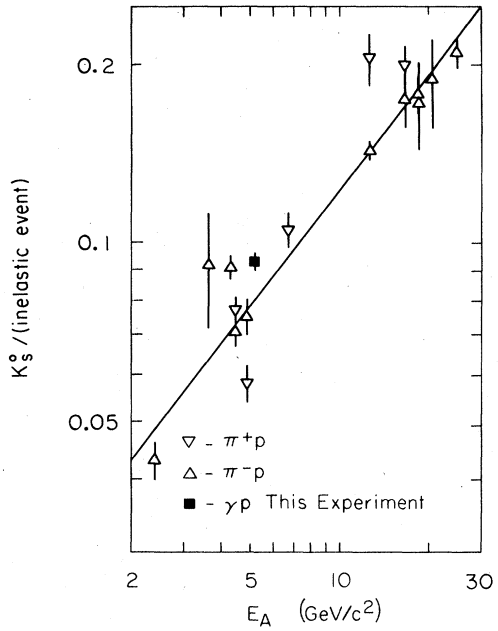

FIG. 4. Number of K_S^0 per inelastic event as a function of the available energy. The straight line is a fit to the π^+p and π^-p data.

does not have. It is clear from the figures that the γp data is consistent with a 10% excess. However, because of the spread of the $\pi^{\pm}p$ data no solid conclusions can be made. If the ρ mass were subtracted from E_A in the photoproduction case or if other vector-meson cross sections were subtracted from the inelastic cross sections, the points would lie further above the $\pi^{\pm}p$ fit lines.

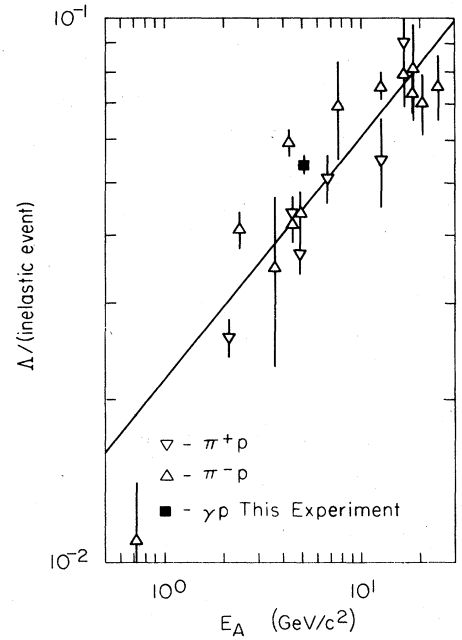

FIG. 5. Number of Λ per inelastic event as a function of the available energy. The straight line is a fit to the π^+p and π^-p data.

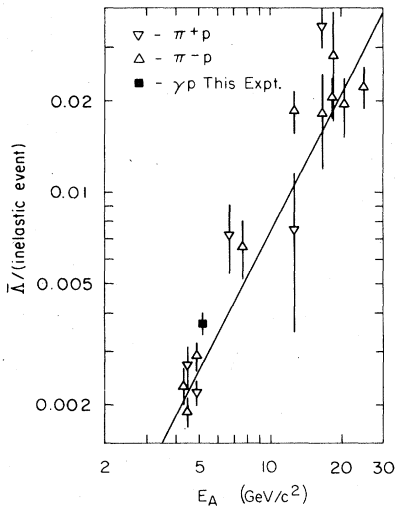

FIG. 6. Number of $\bar{\Lambda}$ per inelastic event as a function of the available energy. The straight line is a fit to the π^+p and π^-p data.

C. Other strange-baryon cross sections

1. Ξ^- selection and cross section

The sample of events used to extract the Ξ^- cross section is the same as that used for the inclusive Λ and $\bar{\Lambda}$ samples. The Ξ^- decays to $\Lambda\pi^- \sim 100\%$ of the time. Requiring both the Λ and the π^- to be visible in the bubble chamber left 594 candidate events with both a neutral V^0 and a charged V^-. These contained 623 V^0V^- combinations.

In order to ensure that a sufficient length of the outgoing tracks was seen in the chamber, each vertex, V^0 and V^-, was required to be at least 11 cm from the bubble-chamber walls. In addition, in order to be sure that the vertices were cleanly separated, the two vertices were required to be at least 0.2 cm apart and the V^- at least 0.2 cm apart from the primary vertex. An acceptance weight, which is the product of the Ξ^- weight and the Λ weight, was applied to each event to correct for these losses.

The unfitted mass for the three outgoing charged tracks of the V^0V^- interpreted as $(p\pi^-)\pi^-$ is shown in Fig. 7. The Ξ^- peak is obvious at 1.321 GeV/c^2 on top of a small background.

In order to remove events with poorly measured decay products, cuts of $\Delta p/p < 0.5$, $\Delta\phi < 0.05$ rad, and $\Delta\lambda < 0.05$ rad were imposed on the momentum, azimuth, and dip uncertainties of the decay products of the V^- and V^0 (interpreted as π^-, p, and π^-, respectively). This removed 23 V^-V^0 combinations. A correction was made for this small loss.

Two more cuts were made to reduce the background. First, the V^0 interpreted as a $p\pi^-$ was required to have an invariant mass within 3σ of the Λ mass (1.115 GeV/c^2). Second, the V^0 was required to point to the decay of the V^- as follows: The V^0 momentum $\mathbf{p}$ was required to be almost collinear with the vector $\mathbf{V}$, connecting the V^- production vertex to the V^0 decay vertex. The angle between the two vectors, $\cos\theta = \mathbf{p}\cdot\mathbf{V}/|\mathbf{p}||\mathbf{V}|$ is shown in

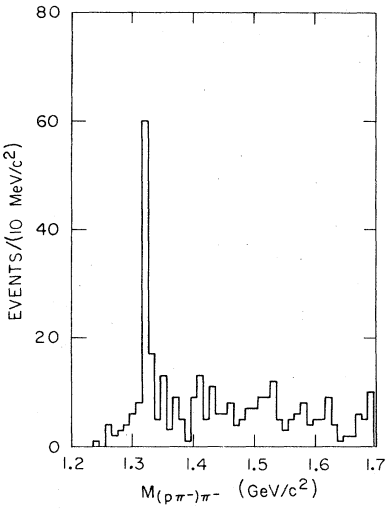

FIG. 7. Unfitted mass of outgoing charged decay products interpreted as $(p\pi^-)\pi^-$ of all V^-V^0 combinations.

Fig. 8(a) for the V^-V^0 combinations that have passed the Λ 3σ cut. Obviously, some events contain V^- and V^0 vertices which are unrelated. A value of $\cos\theta > 0.95$ was therefore required for the V^-V^0 to be kept as a Ξ^-. The $(p\pi^-)\pi^-$ mass combinations after the two cuts is shown in Fig. 8(b). The events with $\cos\theta < 0.95$ have no $M_{(p\pi^-)\pi^-}$ peak in the Ξ^- range. The final Ξ^- sample is taken as those events whose invariant masses are $1.296 < M_{(p\pi^-)\pi^-} < 1.346$ GeV/c^2. There are 73 combinations in this sample. No event has more than one V^-V^0 combination that falls in this mass range and passes all three cuts.

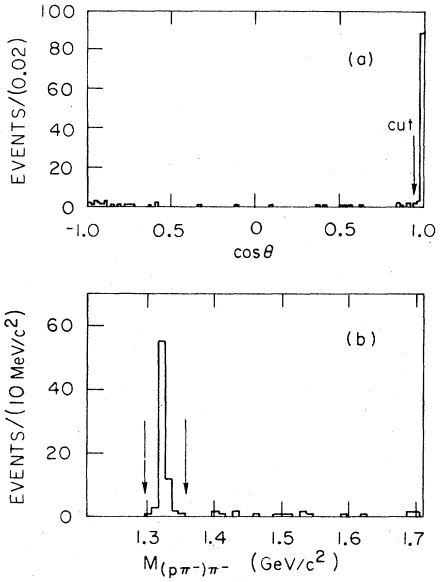

FIG. 8. (a) $\cos\theta$ distribution of Ξ^- candidates, where θ is the angle between the V^0 momentum and the V^-V^0 connector. The cut is at $\cos\theta = 0.95$. (b) Invariant mass of $(p\pi^-)\pi^-$ combinations after the 3σ Λ mass cut and the $\cos\theta$ cut. The arrows show the region kept for further analysis.

A check is made that the three cuts give a number of Ξ^-'s (73) that is consistent with the (signal − background) in the original sample of 546 combinations before cuts (Fig. 7). Taking the two sidebands (where the sidebands are the regions $1.246 < M_{(p\pi^-)\pi^-} < 1.296$ and $1.346 < M_{p\pi^-)\pi^-} < 1.396$) as representative of the background, yields $44/2 = 22$ background events expected in the mass region 1.296–1.346 GeV/c^2. There are 96 entries in this mass region. That leaves $96 - 22 = 74$ real Ξ^- expected. This is consistent with the number (73) that the cuts retain, suggesting that no Ξ^- are lost by the cuts.

The identity of the 73 Ξ^- events was checked by plotting the planarity, the $\cos\theta_{\text{c.m.}}$ distribution, the p_t distribution, and the lifetime of the sample. All of these distributions show consistency with the known characteristics[2] of the Ξ^-.

The cross section for inclusive Ξ^- production is computed by correcting the raw number of events (73) for geometric losses (average weight 1.94), relative trigger efficiency of Ξ^- topology events compared to all hadronic events (0.954), the scanning efficiency for Ξ^- topology events compared to all hadronic events (1.14), and the branching ratio for $\Xi^- \to \Lambda\pi^-$ (1.00) and $\Lambda \to p\pi^-$(0.642). Normalizing the events to the full hadronic sample, the inclusive cross section is $\sigma(\gamma p \to \Xi^- X) = 117 \pm 17$ nb.

As in the K_S^0, Λ, and $\bar{\Lambda}$ cases, the inclusive photoproduction cross section of the Ξ^- has not been measured previously over the full x_F range. The CERN Ω photoproduction experiment has published a value for $\sigma(\gamma p \to \Xi^- X)$ for the limited x_F region $x_F > -0.3$ of 28 ± 9 nb.[10] This can be compared to the value of 94 ± 13 nb found in this experiment in the same x_F region ($x_F > -0.3$). These numbers are clearly inconsistent, especially in view of the probable increase in the Ξ^- cross section with energy. The Ξ^- are measured with completely different techniques in the two experiments. In our experiment, the Ξ^- decays are observed directly and there is very little background. The CERN Ω experiment fits the $\Lambda\pi^-$ mass distribution, which has a very large background in the Ξ^- region.

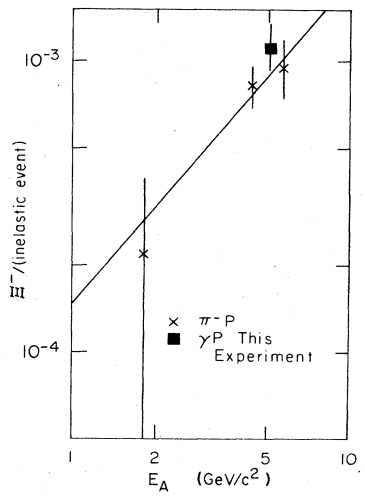

FIG. 9. Number of Ξ^- per inelastic event as a function of available energy. The straight line is a fit to the π^- data.

TABLE IV. Number of Ξ^- per inelastic event for various $\pi^- p$ experiments and this experiment.

Beam	Beam energy (GeV)	E_A (GeV)	$\sigma_{\Xi^-}/\sigma_{\text{inel}}$ ($\times 10^{-3}$)	Reference
π^-	4.00	1.82	0.216±0.172	35
π^-	16.0	4.48	0.821±0.127	36
π^-	25.0	5.84	0.945±0.189	37
γ	19.5	5.18	1.123±0.165	

We compare our Ξ^- data with $\pi^{\pm}p$ data. The ratio of $\sigma(\Xi^-)/\sigma$ (inelastic) for various beam energies in listed in Table IV and shown in Fig. 9. Again, the γp value is higher than the fit to the $\pi^{\pm}p$ data, but there are only three $\pi^{\pm}p$ experiments to compare to, and these are all very low statistics experiments, making detailed comparisons difficult.

2. $\bar{\Xi}^-$ cross section

The $\bar{\Xi}^-$ was searched for in the V^0V^+ topology events. Cuts very similar to those used in the Ξ^- search were made and a sample of 9±4 events was found. Figure 10 shows the unfitted mass of the V^0V^- combinations interpreted as $(\bar{p}\pi^+)\pi^+$ before and after the cuts are made. A $\bar{\Xi}^-$ signal is clear. Correcting for geometric losses, trigger and scan efficiencies, and branching ratios, gives $\sigma(\gamma p \to \bar{\Xi}^- X) = 10 \pm 4$ nb.

3. Σ^0 cross section

The Σ^0 decays to $\Lambda\gamma \sim 100\%$ of the time. Therefore, a search for the Σ^0 was made by using events with more than one V^0 in the fiducial volume (i.e., it was demanded that both the Λ and the γ be seen in the bubble chamber). There were 1530 candidate $\Lambda\gamma$ combinations in this sample. Some of the laboratories collaborating on this experiment did not have the ability to process events with ≥ 3 V^0. In those cases, 2 V^0 were measured and included on the DST. We have corrected for the resulting losses of Σ^0 as described below.

The Λ's were identified by using 3C fits, and ambiguities between Λ/K_S^0 and Λ/γ were resolved in the same way as in the V^0 analysis. For each event, the Λ was paired with all other V^0's in the chamber that were consistent with being γ's. The definition of a γ is also the same here as in the V^0 analysis. There were 468 remaining $\Lambda\gamma$ combinations. For each combination, the invariant mass of the $(p\pi^-)\gamma$ was formed. Figure 11 shows the unweighted mass distribution. A peak is seen at the Σ^0 mass (1192 MeV/c^2).

To calculate a cross section, the Λ is weighted for various losses as in Sec. III B above and the γ is weighted by the inverse of its conversion probability, determined by using energy-dependent cross sections for pair production in hydrogen.[11,12] The weights are fairly large (average 73.6 for the $\Lambda\gamma$ mass range 1180—1200 MeV/c^2), reflecting the low probability for γ conversions in hydrogen. The weighted mass distribution is shown in Fig. 12. Comparison of Figs. 11 and 12 confirms that the average weight does not depend greatly on the $\Lambda\gamma$ mass.

To compute a cross section, the Σ^0 lost due to the 2 V^0 restriction for certain laboratories must be corrected for. The two largest classes of losses arise from the reactions $\gamma p \to \Sigma^0 K_S^0 X$ and $\gamma p \to \Sigma^0 \pi^0 X$. In the first case the Λ (from the Σ^0) and the K_S^0 would be measured but the converted γ neglected. To estimate the maximum size of this loss it will be assumed that the number of visible ΛK_S^0

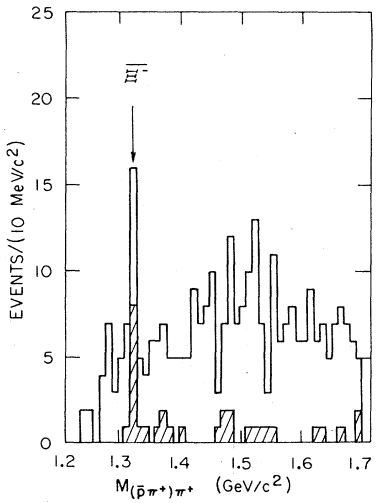

FIG. 10. Unfitted mass of outgoing charged decay products interpreted as $(\bar{p}\pi^+)\pi^+$ of V^+V^0 combinations. The shaded portion is the events left after the cuts are made.

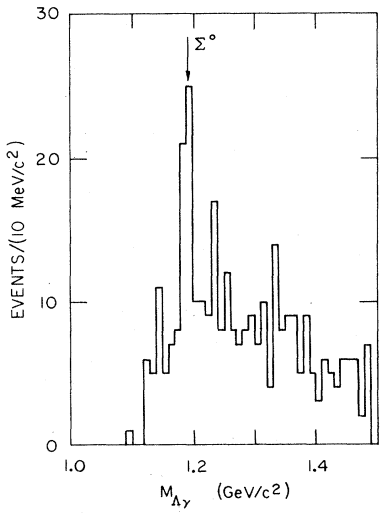

FIG. 11. Unweighted mass distribution of the $\Lambda\gamma$ combinations.

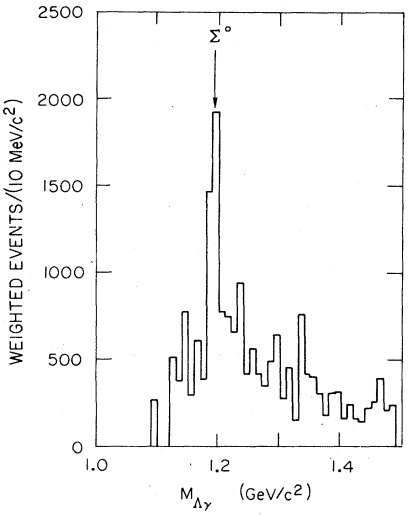

FIG. 12. Weighted mass distribution of the $\Lambda\gamma$ combinations.

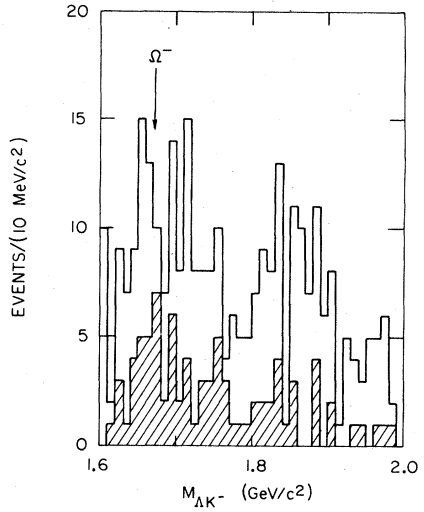

FIG. 13. Invariant mass distribution of V^-V^0 combinations interpreted as ΛK^-. The arrow shows the Ω^- mass position. The shaded portion is the events remaining after the cuts are made (see text).

pairs divided by the total number of visible Λ is approximately equal to the visible $\Sigma^0 K_S^0$ pairs divided by the visible Σ^0, i.e.,

$$\frac{\text{No.}K_S^0\Lambda}{\text{No.}\Lambda}=\frac{\text{No.}\Sigma^0K_S^0}{\text{No.}\Sigma^0}\ .$$

If we assume that all of the visible $\Sigma^0K_S^0$ are lost by these laboratories then there are $(815\pm29)/(7315\pm93)=(11.1\pm0.4)\%$ Σ^0 lost. The second source of loss, $\Sigma^0\pi^0$, is a bit harder to estimate. We will assume that each event has on the average 1 π^0. Folding in the probability of conversion, and assuming that there is a 50% chance of measuring the wrong γ, the probability of losing the Σ^0 is $P=\frac{1}{2}\times P(\gamma)=1.1\%$. Summing the two corrections yields $(12.2\pm0.4)\%$ lost. The cross section for the Σ^0 from the complete laboratories is 1.79 ± 0.74 μb. The corrected cross section for the other laboratories is 1.56 ± 0.56 μb. They agree within errors and can be combined to yield 1.65 ± 0.44 μb.

4. Ω^- *upper limit*

The Ω^- was searched for in the ΛK^- decay channel. Because this topology is the same as the Ξ^- decay topology (V^-V^0), similar cuts can be used here as were used to isolate Ξ^- candidates. The $(p\pi^-)K^-$ invariant-mass plot for all V^0V^- combinations is shown in Fig. 13. No Ω^- signal is seen. After the Λ-mass cut and the Λ-pointing cuts are made (the same cuts as for the Ξ^- sample) the $(p\pi^-)K^-$ invariant-mass plot is given by the shaded portion of Fig. 13. A broad peak is seen at the Ω^- mass (1672 MeV/c^2), but the reflection of the Ξ^- into the Ω^- mass range when the π^- is misassigned the K^- mass must be considered.

In order to estimate the number of Ω^-'s that are ambiguous with Ξ^-, the mass of each candidate interpreted as $(p\pi^-)\pi^-$ is plotted in Fig. 14 versus its mass interpreted as $(p\pi^-)K^-$. The regions between the solid lines represent the Ω^- region $(1.650<M_{(p\pi^-)K^-}<1.700$ GeV/c^2) and the Ξ^- region $(1.300<M_{(p\pi^-)\pi^-}<1.350$ GeV/c^2). A very clear Ξ^- is seen. There are three events in the Ω^- region that fall outside of the Ξ^- region. To estimate the number of Ω^- decays that might be in the Ξ^- region, Ω^- events were generated by a Monte Carlo program and the K^- was assigned the π^- mass to mimic Ξ^- decays. From the scatter plot of $(p\pi^-)K^-$ vs $(p\pi^-)\pi^-$ mass the ratio of Ω^- outside the Ξ^- region to the number inside was found to be 6.6. From the three events that are outside the Ξ^- region, we estimate that $3/6.6=0.5$ events in the Ξ^- region are Ω^-, assuming that all three outside the region are Ω^-. If there are no more than 3.5 events in the Ω^- mass range, then there are no more than 7.3 events at the 90% confidence level (CL),

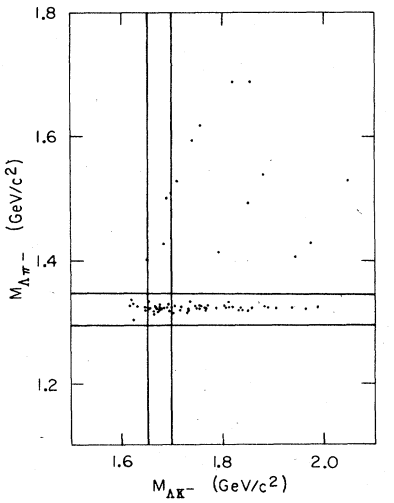

FIG. 14. Invariant mass of V^-V^0 combinations interpreted as $\Lambda\pi^-$ vs ΛK^-. The regions between the solid lines represent the Ω^- mass region (vertical) and the Ξ^- mass region (horizontal).

or $\sigma(\gamma p \to \Omega^- X) < 17.1$ nb (90% CL). The weights, scanning efficiency, and triggering efficiency are all taken to be the same as those used for the Ξ^- cross section calculation. The branching ratio of $\Omega^- \to \Lambda K^-$ of 0.686 is used.

5. $\Sigma^{*\pm}(1385)$ cross sections

The $\Sigma^*(1385)$ was searched for in the $\Lambda\pi^\pm$ decay channels. All unique and resolved Λ's are used in the search for the $\Sigma^*(1385)$. Each of the Λ's is paired with every charged track originating at the primary vertex and not decaying in the chamber. Figures 15 and 16 show the weighted $\Lambda\pi^+$ and $\Lambda\pi^-$ mass distributions. The events are weighted for the Λ geometric acceptance, etc., as for the Λ inclusive events. A clear $\Sigma^*(1385)$ signal is seen in each channel. Each mass distribution is fit to a Gaussian plus background. The Gaussian is fixed with its center at the $\Sigma^*(1385)$ mass (1382 MeV for Σ^{*+} and 1387 MeV for Σ^{*-}) with a width of 30 MeV/c^2. The background shape is parametrized as $a(M-M_{\rm th})^b e^{-cM}$, where $M_{\rm th}=M_\Lambda+M_\pi$ is the threshold invariant mass of the $\Lambda\pi$. The fits give (208 ± 19) Σ^{*+} and (109 ± 15) Σ^{*-} unweighted events. The fits are shown in Figs. 15 and 16 as solid lines. The dotted lines show the fitted background shape under the signal.

Correcting for trigger acceptance and losses of Λ's and for the branching ratios of $\Sigma^* \to \Lambda\pi$ (0.88 ± 0.02) and $\Lambda \to p\pi^-$ (0.642), gives the cross sections tabulated in Table II. The $\Sigma^*(1385)$ cross sections agree very well with the results of a previous analysis of this experiment.[1]

D. Pair cross sections

The cross sections for $\gamma p \to K_S^0 K_S^0 X$, $\gamma p \to K_S^0 \Lambda X$, $\gamma p \to K_S^0 \bar{\Lambda} X$, and $\gamma p \to \Lambda\bar{\Lambda} X$ were measured using V^0's restricted to the clean kinematic ranges in $\cos\theta_{\rm c.m.}$ (defined in Sec. IV A below). The pair cross sections were corrected for losses, scan, and trigger efficiencies, and the branching ratios as discussed above for single-particle inclusive cross sections. Table II gives the results. An indication of the efficiency of these cuts for separating ambiguous decays into K_s^0 and Λ is that there are only four events interpreted as $\Lambda\Lambda$ compared to 366 interpreted as $K_s^0\Lambda$.

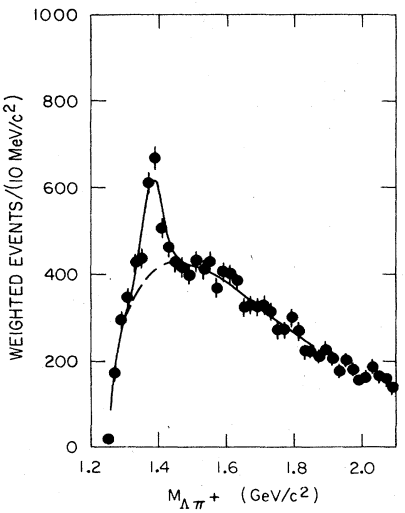

FIG. 15. Weighted mass distribution of $\Lambda\pi^+$ combinations. The solid curve is the overall fit (signal + background). The dashed line is the background shape as described in the text.

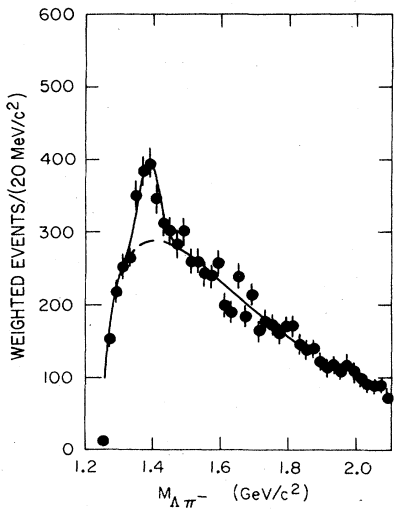

FIG. 16. Weighted mass distribution of $\Lambda\pi^-$ combinations. The solid curve is the overall fit (signal + background). The dashed line is the background shape as described in the text.

Some observations can be made about the pair cross sections. The $K_S^0K_S^0$ pair production and the $K_S^0\Lambda$ associated cross sections are of comparable size. Λ's are produced with K_S^0 much more often than with $\bar{\Lambda}$. The $\Lambda\bar{\Lambda}$ cross section is small compared to the pair or associated cross sections and is 2.2% of the total inclusive Λ cross section. In contrast, about $\frac{1}{3}$ of the $\bar{\Lambda}$ inclusive cross section can be accounted for by $\Lambda\bar{\Lambda}$ production, whereas only $\sim$6% of the $\bar{\Lambda}$ are produced via $K_S^0\bar{\Lambda}$ associated production.

IV. FEYNMAN-x DISTRIBUTIONS AND COMPARISONS TO A QUARK-DIQUARK FUSION MODEL

A. x_F distributions

The x_F distributions are computed using a limited subsample of the V^0's. To provide a clean sample of K_S^0, Λ, and $\bar{\Lambda}$ the distributions were computed with V^0's in the following $\cos\theta_{\rm c.m.}$ regions:

Particle	Range
K_S^0	$-0.8 < \cos(\theta_{\rm c.m.}) < 0.8$
Λ	$-1.0 < \cos(\theta_{\rm c.m.}) < 0.1$
$\bar{\Lambda}$	$-0.1 < \cos(\theta_{\rm c.m.}) < 1.00$

This choice of regions reduces the maximum possible background from misidentified ambiguous events to 0.3%, 1.1%, and 8.9% for the K_S^0, Λ, and $\bar{\Lambda}$ samples, respectively. The Ξ^- distribution was computed with a cut of $\cos\theta_{\rm c.m.} < 0.8$. This was necessary because of possible losses in the $\cos\theta_{\rm c.m.} > 0.8$ region, where the Ξ^- kink

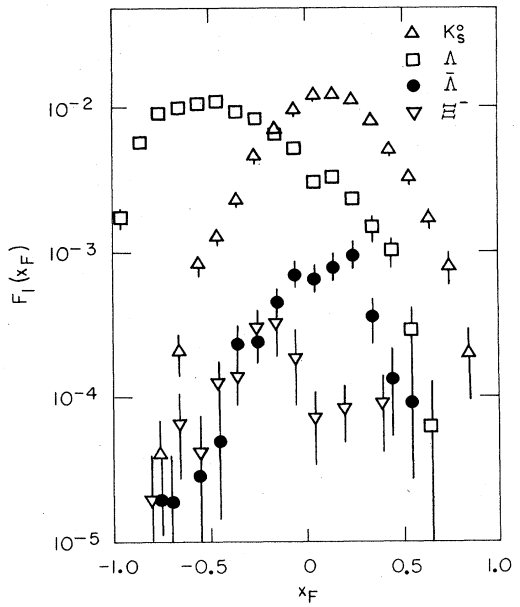

FIG. 17. $F_1(x_F)=(1/\sigma_T)(2E/\pi\sqrt{s})(d\sigma/dx_F)$ distribution of inclusive K_S^0, Λ, $\bar{\Lambda}$, and Ξ^-.

angle is smallest.

The invariant Feynman-x distributions

$$F_1(x)=\frac{1}{\sigma_T}\frac{2E}{\pi\sqrt{s}}\frac{d\sigma}{dx}$$

are plotted in Fig. 17. Here, $x_F=2p_L^{\text{c.m.}}/\sqrt{s}$, E is the energy of the V^0 in the overall γp center of mass, σ_T is the total photoproduction cross section and s is the invariant mass squared of the γp system $=37.5$ GeV.[2]

Note that x_F is calculated using a $\sqrt{s}$ that assumes a beam energy of 19.5 GeV. The beam energy spread contributes an error of $\pm 5\%$ to the x_F so defined.

The distributions in Fig. 17 show the following characteristics. The K_S^0 is centrally peaked. The Λ distribution is peaked strongly in the backward direction ($x_F<0$), which is expected if the Λ carries on average $\frac{2}{3}$ of the target proton's ($x_F=-1$) quarks. The $\bar{\Lambda}$ is centrally peaked. This is also expected because the three valence quarks in the $\bar{\Lambda}$ are antiquarks and hence cannot come from the valence quarks of the proton. The Ξ^-, having one quark in common with the proton, is expected to peak at $x_F\sim-\frac{1}{3}$, which it does.

B. The quark-diquark fusion model

The x_F distributions of strange-baryon production can be modeled by a quark-diquark fusion mechanism.[13] In this model the strange baryon S_b produced in the reaction $\gamma p\to S_b+X$, is the product of the "fusion" of a quark from one initial-state particle and a diquark from the other initial-state particle (Fig. 18). This fusion model is analogous to the Drell-Yan production of dilepton pairs in hadron-hadron scattering.

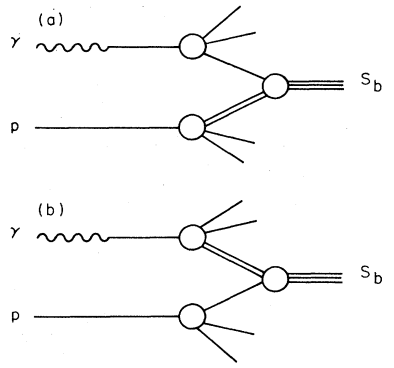

FIG. 18. Quark-diquark fusion in photoproduction. (a) Contribution from a quark from the photon (vector meson) and a diquark from the proton. (b) Contribution from a diquark from the photon (vector meson) and a quark from the proton.

1. Assumptions

The assumptions of the model are the following.

(1) The valence-quark flavors of the produced baryon consist of the quark flavors of the quark and diquark involved in the fusion.

(2) Quarks can be valence or sea quarks.

(3) Diquarks are composed of two valence quarks (valence diquark) or a valence and a sea quark (sea diquark). Diquarks containing only sea quarks are assumed not to contribute to the fusion process.

(4) Antiquarks can be valence or sea antiquarks.

(5) Antidiquarks consist of one valence antiquark and one sea antiquark (sea antidiquark).

The subject of quark structure functions within the photon has been treated by many authors.[14–16] The photon can be considered to consist of a pointlike part (which can be calculated in QCD) and a hadronlike part, which can be computed using the vector-meson dominance model (VDM).

It will be assumed that only the VDM piece contributes to the quark structure functions in this experiment. This is a reasonable assumption in light of the success that VDM gives in explaining many of the other facets of photoproduction with real photons.[8] This gives the following form of the structure function:

$$F_\gamma(x)=\sum_i\left[\frac{4\pi\alpha}{\gamma_i^2}\right]F_i(x)\ ,$$

where x is the momentum fraction of a particular parton in the photon (or vector meson), and the summation is over the vector mesons coupling to the photon.

In evaluating the $F_i(x)$ we assume only the ρ, ω, and ϕ vector mesons contribute significantly. The ρ and ω meson structure functions are both considered to be an average over π^+ and π^- structure functions:

$$F_\rho(x)=\frac{4\pi\alpha}{\gamma_\rho^2}\frac{1}{2}[F_{\pi^+}(x)+F_{\pi^-}(x)]\ ,$$

$$F_\omega(x)=\frac{4\pi\alpha}{\gamma_\omega^2}\frac{1}{2}[F_{\pi^+}(x)+F_{\pi^-}(x)]\ .$$

TABLE V. Structure functions of the pion.

Pion valence quark	$V_\pi^q(x)=0.64x(1-x)$	$x\geq 0.5$
	$V_\pi^q(x)=0.32x^{1/2}(1-x)^{1/2}$	$x\leq 0.5$
Pion sea quark(antiquark)	$S_\pi^q(x)=0.19(1-x)^5$	
Pion sea diquark (antidiquark)	$S_\pi^{qq}(x)=(1-x)^3$	

TABLE VI. Structure functions of the proton.

Proton valence quark	$V_p^q(x)=2.66x(1-x)^3$	$x\geq 0.25$
	$V_p^q(x)=0.86x^{1/2}(1-x)^{3/2}$	$x\leq 0.25$
Proton valence diquark	$V_p^{qq}(x)=x^2(1-x)$	
Proton sea diquark	$S_p^{qq}(x)=(1-x)^5$	
Proton sea quark (antiquark)	$S_p^q(x)=0.20(1-x)^7$	

The ϕ is considered to be $s\bar{s}$ as far as valence-quark content is concerned, but the shape of the structure functions is that of the π structure functions. These are reasonable assumptions because the ϕ has $q\bar{q}$ structure and the quark-counting rules, from which many of the structure function shapes are derived, predict shapes based on the number of valence constituents, independent of flavor.

The π structure function is assumed to consist of both valence and sea terms. The shapes, as given by Donnachie,[13] are given in Table V.

Theoretically, the charge couplings of the quarks in the vector mesons to the photon are the ratio $4\pi/\gamma_\rho{}^2:4\pi/\gamma_\omega{}^2:4\pi/\gamma_\phi{}^2=9:1:2$. Measurements of these couplings have been made in photoproduction and in colliding-beam experiments. The extraction of the couplings from photoproduction data requires making some assumptions about the real-to-imaginary parts ratio of the $\gamma p\to Vp$ cross sections and the values of $\sigma(Vp)$, where $V=$ a vector meson. Depending on the set of assumptions used, the ratios vary (see Table 11 of Ref. 17) from 9:0.7:0.5 to 9:1.14:2.15. The colliding-beam experiments measure the widths of the vector mesons and extract the coupling constants directly. These yield a $\rho{:}\omega{:}\phi$ ratio of $9:1.04\pm0.18:1.41\pm0.24$.[17]

In this analysis, we take $\gamma_\rho{}^2/4\pi=2.39\pm0.02$, a value determined in a recent high-statistics photoproduction experiment at energies near ours.[18] This value agrees with earlier results.[17] We fix the $\rho{:}\omega{:}\phi$ ratio at 9:1:2. The effect of a different ratio will be shown when the fits are discussed.

The structure functions of the proton are also given by Donnachie[13] and are listed in Table VI.

Starting from the Drell-Yan formula for dilepton production in hadron-hadron collisions, the following formula can be derived[2] for the x_F distribution of inclusive baryon photoproduction:

$$\frac{1}{\sigma_T}\frac{2E}{\pi\sqrt{s}}\frac{d\sigma}{dx_F}=\frac{1}{\sigma_T\pi}\frac{4\pi^2}{3M^2}\frac{g^2}{4\pi}[F_\gamma^g(x_1)F_p^{qq}(x_2)+F_\gamma^{qq}(x_1)F_p^q(x_2)]\ ,$$

where $g^2/4\pi$ is the unknown fusion coupling constant, σ_T the total hadronic photoproduction cross section, M^2 the mass squared of the strange baryon produced, and the structure functions are defined in terms of π and proton structure functions, where

$$F_\pi^q(x)=V_\pi^q(x)+S_\pi^q(x)\ ,$$
$$F_p^q(x)=V_p^q(x)+S_p^q(x)\ ,$$
$$F_\pi^{qq}(x)=S_\pi^{qq}(x)\ ,$$
$$F_p^{qq}(x)=V_p^{qq}(x)+S_p^{qq}(x)\ .$$

Here the V's are the valence-quark or diquark structure functions and the S's are the sea-quark or diquark structure functions.

C. Fits to data

1. Λ *fits*

The Λ consists of valence (uds) and can be formed by quark-diquark combinations of the forms $u(ds)$, $d(us)$, and $s(ud)$. Consider first the $u(ds)$ form. As one example, the u quark can be a valence u from the proton. In such a case the (ds) diquark must be a sea diquark from the photon. Thus the form is $s_\pi^{qq}S_\pi^{qq}(x_1)V_p^q(x_2)$, where s_π^{qq} is an unknown coefficient of the diquark structure function. The other combinations can be found in a similar way. The numerical coefficients are determined by adding up all the possible ways to form (uds) combinations.

The Feynman x distribution for the Λ, with all of its numerical factors, is

$$\begin{aligned}\frac{1}{\sigma_T}\frac{2E}{\pi\sqrt{s}}\frac{d\sigma}{dx_F}=&\frac{1}{\sigma_T}\frac{4\pi\alpha}{3M^2}\frac{g^2}{4\pi}\left[\left(\frac{\gamma_\rho{}^2}{4\pi}\right)^{-1}+\left(\frac{\gamma_\omega{}^2}{4\pi}\right)^{-1}\right][v_p^{qq}S_\pi^q(x_1)V_p^{qq}(x_2)+\tfrac{3}{2}s_\pi^{qq}S_\pi^{qq}(x_1)V_p^q(x_2)\\&+2s_\pi^{qq}S_\pi^{qq}(x_1)S_p^q(x_2)+s_p^{qq}V_\pi^q(x_1)S_p^{qq}(x_2)\\&+4s_p^{qq}S_\pi^q(x_1)S_p^{qq}(x_2)]\\&+\frac{1}{\sigma_T}\frac{4\pi\alpha}{3M^2}\frac{g^2}{4\pi}\left[\frac{\gamma_\phi{}^2}{4\pi}\right]^{-1}[v_p^{qq}S_\pi^q(x_1)V_p^{qq}(x_2)+3s_\pi^{qq}S_\pi^{qq}(x_1)V_p^q(x_2)\\&+2s_\pi^{qq}S_\pi^{qq}(x_1)S_p^q(x_2)+2s_p^{qq}V_\pi^q(x_1)S_p^{qq}(x_2)\\&+4s_p^{qq}S_\pi^q(x_1)S_p^{qq}(x_2)+v_p^{qq}V_\pi^q(x_1)V_p^{qq}(x_2)]\ .\end{aligned}$$

TABLE VII. (a) Results of the fits to Λ, $\bar{\Lambda}$, and Ξ^- x_F distributions using 9:1:2 as the ρ:ω:ϕ ratio. (b) Results of the fits to Λ, $\bar{\Lambda}$, and Ξ^- data using 9:1:1.4 as the ρ:ω:ϕ ratio.

(a)

	Λ	$\bar{\Lambda}$	Ξ^-
$(g^2/4\pi)v_p^{qq}$	8.74±0.21		
$(g^2/4\pi)s_\pi^{qq}$	0.244±0.009	0.329±0.020	0.187±0.012
$(g^2/4\pi)s_p^{qq}$	0.0	0.0	0.0
χ^2/DF	21/14	47/12	14/9

(b)

	Λ	$\bar{\Lambda}$	Ξ^-
$(g^2/4\pi)v_p^{qq}$	9.35±0.30		
$(g^2/4\pi)s_\pi^{qq}$	0.269±0.012	0.347±0.023	0.241±0.040
$(g^2/4\pi)s_p^{qq}$	0.0	0.0	0.0
χ^2/DF	21/14	47/12	16/9

A χ^2 fit was made to the Λ data with the resultant coefficients listed in Table VII(a).

It is interesting to note that there are two types of terms in the formula that involve the coefficient s_π^{qq}, those with $S_\pi^{qq}S_p^q$ and those with $S_\pi^{qq}V_p^q$. The distribution was also fitted assuming that these are independent coefficients. The fit gave a first term of $(g^2/4\pi)s_\pi^{qq}=0.232\pm0.017$ while the second was $(g^2/4\pi)s_\pi^{qq}=0.238\pm0.066$. These two numbers agree well, as predicted by the model.

The result of the fit is plotted in Fig. 19. The five curves show the contributions from the four different shapes that contribute plus the sum of the four. We note that in the formula above more than one curve can correspond to a single coefficient. For example, the second and third terms, $\frac{3}{2}s_\pi^{qq}S_\pi^{qq}(x_1)V_p^q(x_2)$ and $2s_\pi^{qq}S_\pi^{qq}(x_1)S_p^q(x_2)$, have the same coefficient s_π^{qq} but have completely different shapes (long dash and short dash curve, respectively, on Fig. 19). The fit is very good across the entire x_F range, with the possible exception of the high-x_F points.

A possible explanation of the discrepancy of the fit from the data in the high-x_F range lies in the production and decay of resonances, which have been ignored up to this point. For example, the Σ^0 decays to Λ and γ and the $\Sigma^*(1385)$ decays to Λ and π. In both of these cases, the Λ is slightly slower in the laboratory (has lower absolute x_F) than the parent Σ. This will lead to a slight softening of the x_F distribution. This model predicts a Σ^0 x_F shape that is identical to the Λ x_F shape for primary Λ and Σ^0 due to the identical quark content of the two baryons. Within the limited statistics, the Σ^0 and Λ x_F distributions agree (not shown).

2. $\bar{\Lambda}$ *fits*

The $\bar{\Lambda}$ has three valence antiquarks. The proton cannot contribute an antidiquark in this model. Therefore, the photon is the source of the sea antidiquark and the antiquark arises from the sea of the proton. The predicted distribution is

$$\frac{1}{\sigma_T}\frac{2E}{\pi\sqrt{s}}\frac{d\sigma}{dx_F} = \frac{1}{\sigma_T}\frac{4\pi\alpha}{3M^2}\frac{g^2}{4\pi}\left[\left[\frac{\gamma_\rho^2}{4\pi}\right]^{-1}+\left[\frac{\gamma_\omega^2}{4\pi}\right]^{-1}+\left[\frac{\gamma_\phi^2}{4\pi}1\right]^{-1}\right] \times[2s_\pi^{qq}S_\pi^{qq}(x_1)S_p^q(x_2)] .$$

A χ^2 fit was made to the $\bar{\Lambda}$ data, yielding $(g^2/4\pi)s_\pi^{qq}=0.329\pm0.020$ for a χ^2/DF of 47/12. The fitted distribution plotted in Fig. 20 follows the general characteristics of the data but is significantly higher at large x_F.

3. Ξ^- *fits*

The form of the invariant Feynman-x distribution is

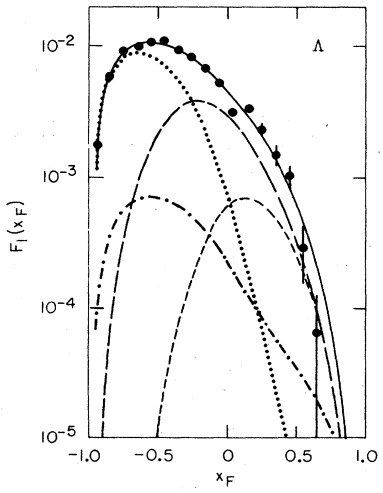

FIG. 19. Fit of the quark-diquark fusion model to the Λ inclusive distribution. The curves show the contributions from: dotted, $S_\pi^q V_p^{qq}$; long dash, $S_\pi^{qq}V_p^q$; short dash, $S_\pi^{qq}S_p^q$; dot-dash, $V_\pi^q V_p^{qq}$; and solid, sum of the four.

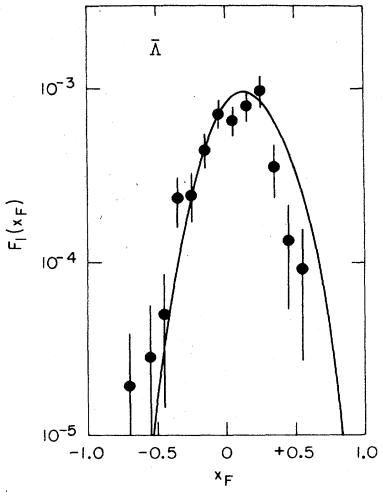

FIG. 20. Fit of the quark-diquark fusion model to the $\bar{\Lambda}$ inclusive distribution. Only terms of the form $S_\pi^{qq}S_p^q$ contribute.

$$\frac{1}{\sigma_T}\frac{2E}{\pi\sqrt{s}}\frac{d\sigma}{dx_F}=\frac{1}{\sigma_T}\frac{4\pi\alpha}{3M^2}\frac{g^2}{4\pi}\left[\left[\frac{\gamma_\rho{}^2}{4\pi}\right]^{-1}+\left[\frac{\gamma_\omega{}^2}{4\pi}\right]^{-1}\right][\tfrac{1}{2}s_\pi^{qq}S_\pi^{qq}(x_1)S_p^q(x_2)+s_p^{qq}S_\pi^q(x_1)S_p^{qq}(x_2)]$$
$$+\frac{1}{\sigma_T}\frac{4\pi\alpha}{3M^2}\frac{g^2}{4\pi}\left[\frac{\gamma_\phi{}^2}{4\pi}\right]^{-1}[2s_\pi^{qq}S_\pi^{qq}(x_1)S_p^q(x_2)+s_p^{qq}S_\pi^q(x_1)S_p^{qq}(x_2)+s_p^{qq}V_\pi^q(x_1)S_p^{qq}(x_2)$$
$$+s_\pi^{qq}S_\pi^{qq}(x_1)V_p^q(x_2)]\,.$$

A χ^2 fit was made to the Ξ^- data yielding the coefficients listed in Table VII(a) and shown in Fig. 21. The χ^2/DF is 14/9. This fit adequately describes the entire x_F range.

4. *Discussion of the quark-diquark fusion-model fit results*

Several observations can be made about the results of the fits of the quark-diquark fusion model to Λ, $\bar{\Lambda}$, and Ξ^- production. First, the model describes reasonably well the x_F shapes of Λ, $\bar{\Lambda}$, and Ξ^- as well as the relative cross-section magnitudes of the three particles. It does so with a consistent set of parameters and with structure functions identical to those used for describing $\pi^\pm p$ and pp ($\bar{p}p$) strange-baryon production.[13]

The Λ cross section is by far the largest of the three, dominated by the v_p^{qq} terms corresponding to a valence (ud) diquark from the proton and a valence or sea s quark from the photon. The x_F distribution of the Λ peaks in the backward direction, reflecting the strongly negative x_F shape of the proton (ud) valence diquark. The shapes of the primary Σ^0 and Λ (i.e., those that are not decay products of higher-mass states) should be the same in the model. The data show the Λ and Σ^0 shapes to be compatible.

The contributions of s_π^{qq} to Λ, $\bar{\Lambda}$, and Ξ^- are similar in magnitude as predicted by the model. The values are listed in Table VII(a). However, the coefficient is $\sim$30% larger for $\bar{\Lambda}$ than for Λ and for Ξ^- it is about 25% smaller. It is possible that the γ couples directly to $\Lambda\bar{\Lambda}$ or to $s\bar{s}$ for some fraction of the produced Λ and $\bar{\Lambda}$. This part of the production is not explained by the quark-diquark fusion model. Since we are forcing the model to fit all Λ and $\bar{\Lambda}$ production, this causes the $\bar{\Lambda}$ coefficient to be larger than the Λ coefficient. (The effect is relatively much larger for $\bar{\Lambda}$ than Λ because the Λ cross section section is much larger than the $\bar{\Lambda}$ cross section.) The heavier s-quark mass may account for the suppression of Ξ^- production relative to Λ.

The results of fitting the data with a different value of the ratio, 9:1:1.4 (rather than 9:1:2), is given in Table VII(b). The $\Xi^- s_\pi^{qq}$ value changes the most, increasing by 30%, while the Λ and $\bar{\Lambda}$ s_π^{qq} increase less. Thus, part of the departure from equality of the s_π^{qq} coefficients may be attributable to the not-well-known $\rho{:}\omega{:}\phi$ ratio.

It is also found that no contribution of the s_p^{qq} term is needed to fit the Λ or Ξ^- distribution; i.e., no contribution from the sea diquark of the proton is needed to fit the x_F distributions.

The ϕ component of the photon is needed to give good fits to the x_F distributions. In particular, the Ξ^- fit without the ϕ contribution is very poor. Figure 22 shows the result of the fit to the Ξ^- without any ϕ contribution. The χ^2/DF increases from 14/9 in the case when the ϕ is used to 107/9 when it is not. For the Λ and $\bar{\Lambda}$ the ϕ contribution is relatively smaller, but again the fits are improved by its inclusion.

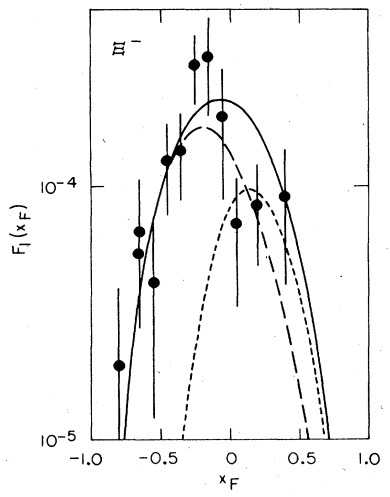

FIG. 21. Fit of the quark-diquark fusion model to the Ξ^- inclusive distribution. The curves show the contributions from: long dash, $S_\pi^{qq}V_p^q$; short dash, $S_\pi^{qq}S_p^q$; and solid, sum of the two.

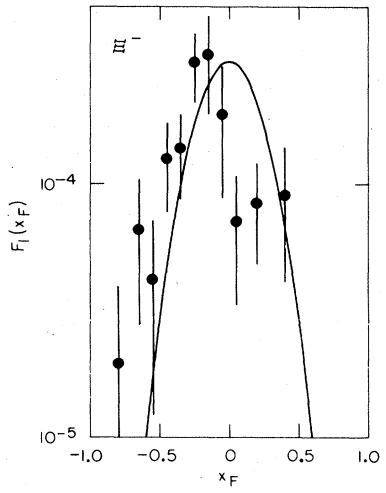

FIG. 22. Fit of the quark-diquark fusion model to the Ξ^- distribution when no ϕ contribution is allowed in the fit.

V. CONCLUSIONS

The cross sections for inclusive K_S^0, Λ, $\bar{\Lambda}$, Ξ^-, $\bar{\Xi}^-$, Σ^0, and $\Sigma^{*\pm}(1385)$ and an upper limit to Ω^- photoproduction at 20 GeV have been measured and are listed in Table II. The K_S^0, Λ, $\bar{\Lambda}$, and Ξ^- rates per inelastic event were compared with $\pi^{\pm}p$ rates and show evidence of an excess which may be due to the $s\bar{s}$ component of the photon.

The pair cross sections were measured and are listed in Table II. The $K_S^0K_S^0$ pair and $K_S^0\Lambda$ associated cross sections are approximately equal. Only a small fraction of Λ production is with $\bar{\Lambda}$ whereas $\sim\frac{1}{3}$ of $\bar{\Lambda}$ production is with Λ.

The x_F distributions of the Λ, $\bar{\Lambda}$, and Ξ^- were presented and compared with the predictions of a quark-diquark fusion model. The model fits the three distributions well with consistent values of the free parameters $(g^2/4\pi)s_{\pi}^{qq}$ etc. The dominant term in Λ production has the coefficient $(g^2/4\pi)v_p^{qq}$ and measures the contribution from the valence diquark in the proton. A smaller contribution arises from the term with coefficient $(g^2/4\pi)s_{\pi}^{qq}$, which measures the sea-diquark contribution from the photon. The sea-diquark contributions from the proton are consistent with zero. It is found that the ϕ (or $s\bar{s}$) component of the photon is needed to fit the x_F distributions well. Without such a piece, the χ^2 increases in all cases, with a large increase for the Ξ^- fit.

ACKNOWLEDGMENTS

We are grateful for the efforts of the SLAC bubble-chamber crew and of the film-scanning and measuring personnel at the participating institutions. We also wish to thank T. Fieguth, R. Gearhart, and J. Murray for setting up the beam lines that made this experiment possible. This work was supported in part by the Department of Energy, Contract DE-AC03-76SF00515, the Japan-U.S. Cooperative Research Project on High Energy Physics under the Japanese Ministry of Education, Science and Culture; the UK Science and Engineering Research Council; the U.S. National Science Foundation.

*Present address: CERN, Geneva, Switzerland.
†Present address: American Dade Co., Costa Mesa, CA 92660.
‡Present address: Fermilab, P.O. Box 500, Batavia, IL 60510.

[1]K. Abe *et al.*, Phys. Rev. D **29**, 1877 (1984).
[2]S. Wolbers, Ph.D. thesis, University of California, Berkeley, 1984, Report No. UCPPG/84/11/08. Many of the details of the analysis and a derivation of the quark-diquark formulas are found here.
[3]C. G. Wohl *et al.*, Particle Data Group, Rev. Mod. Phys. **56**, S1 (1984).
[4]D. O. Caldwell *et al.*, Phys. Rev. Lett. **40**, 1222 (1978).
[5]R. Erbe *et al.*, Phys. Rev. **188**, 2060 (1969).
[6]H. H. Bingham, *et al.*, Phys. Rev. D **8**, 1277 (1973).
[7]D. Aston *et al.*, Nucl. Phys. **B195**, 189 (1982).
[8]T. H. Bauer, R. D. Spital, D. R. Yennie, and F. M. Pipkin, Rev. Mod. Phys. **50**, 261 (1978).
[9]A. P. T. Palounek, Ph.D. thesis, Duke University, 1984.
[10]D. Aston *et al.*, Nucl. Phys. **B198**, 189 (1982).
[11]Y. Tsai, Rev. Mod. Phys. **46**, 815 (1974).
[12]J. H. Hubbell, National Bureau of Standards Report No. NSRDS-NBS29, 1969 (unpublished).
[13]A. Donnachie, Z. Phys. C **4**, 161 (1980).
[14]L. M. Jones *et al.*, Phys. Rev. D **20**, 2749 (1979).
[15]J. Busenitz and J. D. Sullivan, Phys. Rev. D **24**, 1794 (1981).
[16]C. Peterson *et al.*, Nucl. Phys. **B174**, 424 (1980).
[17]D. W. G. S. Leith, *Electromagnetic Interactions of Hadrons* (Plenum, New York and London, 1978), Vol. 1, p. 345.
[18]P. Callahan *et al.*, Report No. FERMILAB-Pub-84/36-E, 1984 (unpublished).
[19]D. Z. Toet *et al.*, Nucl. Phys. **B63**, 248 (1973).
[20]P. Bosetti *et al.*, Nucl. Phys. **B94**, 21 (1975).
[21]P. H. Stuntebeck *et al.*, Phys. Rev. D **9**, 608 (1974).
[22]I. V. Ajinenko *et al.*, Nucl. Phys. **B165**, 1 (1980).
[23]M. Alston-Garnjost *et al.*, Phys. Rev. Lett. **35**, 142 (1975).
[24]D. Brick *et al.*, Nucl. Phys. **B164**, 1 (1980).
[25]J. L. Brown *et al.*, Phys. Rev. **107**, 906 (1957).
[26]R. Sugahara *et al.*, Nucl. Phys. **B156**, 237 (1979).
[27]T. Ferbel and H. Taft, Nuovo Cimento **28**, 1214 (1963).
[28]F. Barriero *et al.*, Phys. Rev. D **17**, 669 (1978).
[29]E. Balea *et al.*, Nucl. Phys. **B163**, 21 (1980).
[30]S. V. Dzmukhadze *et al.*, Yad. Fiz. **31**, 403 (1980) [Sov. J. Nucl. Phys. **31**, 210 (1980)].
[31]N. N. Biswas *et al.*, Nucl. Phys. **B167**, 147 (1980).
[32]D. Brick *et al.*, Phys. Rev. D **20**, 2123 (1979).
[33]D. Ljung *et al.*, Phys. Rev. D **15**, 3163 (1977).
[34]D. Bogert *et al.*, Phys. Rev. D **16**, 2098 (1977).
[35]J. Bartsch *et al.*, Nuovo Cimento **43A**, 1010 (1966).
[36]E. Balea *et al.*, Nucl. Phys. **B150**, 345 (1979).
[37]J. W. Waters *et al.*, Nucl. Phys. **B17**, 445 (1970).